Nitrogen and sulfur for phosphorus: Lipidome adaptation of anaerobic sulfate-reducing bacteria in phosphorus-deprived conditions

Su Ding, Vincent Grossi, Ellen C Hopmans, Nicole J Bale, Cristiana Cravo-Laureau, Jaap S Sinninghe Damsté

PNAS RESEARCH ARTICLE | MICROBIOLOGY OPEN ACCESS

Nitrogen and sulfur for phosphorus: Lipidome adaptation of anaerobic sulfate-reducing bacteria in phosphorus-deprived conditions

Su Ding[a,1], Vincent Grossi[b,2], Ellen C. Hopmans[a], Nicole J. Bale[a], Cristiana Cravo-Laureau[c], and Jaap S. Sinninghe Damsté[a,d]

Edited by Roger Summons, Massachusetts Institute of Technology, Cambridge, MA; received January 18, 2024; accepted May 2, 2024

Understanding how microbial lipidomes adapt to environmental and nutrient stress is crucial for comprehending microbial survival and functionality. Certain anaerobic bacteria can synthesize glycerolipids with ether/ester bonds, yet the complexities of their lipidome remodeling under varying physicochemical and nutritional conditions remain largely unexplored. In this study, we thoroughly examined the lipidome adaptations of *Desulfatibacillum alkenivorans* strain PF2803^T, a mesophilic anaerobic sulfate-reducing bacterium known for its high proportions of alkylglycerol ether lipids in its membrane, under various cultivation conditions including temperature, pH, salinity, and ammonium and phosphorous concentrations. Employing an extensive analytical and computational lipidomic methodology, we identified an assemblage of nearly 400 distinct lipids, including a range of glycerol ether/ester lipids with various polar head groups. Information theory-based analysis revealed that temperature fluctuations and phosphate scarcity profoundly influenced the lipidome's composition, leading to an enhanced diversity and specificity of novel lipids. Notably, phosphorous limitation led to the biosynthesis of novel glucuronosylglycerols and sulfur-containing aminolipids, termed butyramide cysteine glycerols, featuring various ether/ester bonds. This suggests a novel adaptive strategy for anaerobic heterotrophs to thrive under phosphorus-depleted conditions, characterized by a diverse array of nitrogen- and sulfur-containing polar head groups, moving beyond a reliance on conventional nonphospholipid types.

lipidome adaptation | sulfate-reducing bacteria | molecular network | phosphorus limitation

Significance

An essential boundary between bacteria and the environment is their lipid membrane, typically consisting of a fatty acid bilayer bound to glycerol-3-phosphate backbone via ester linkages. However, a number of bacteria also use ether bonds to build their membrane, although the physicochemical factors and nutrient stress affecting their membrane remain elusive. We show that temperature and phosphorus limitation are key to the lipidome adaptation of the mesophilic anaerobic bacterium *Desulfatibacillum alkenivorans*, where the membrane comprises ca. 70 to 90% ether lipids. Under phosphorus limitation, *D. alkenivorans* replaces phospholipids with significant numbers of sulfur-aminolipids for survival. This transformation provides a unique system to explore how a bacterium can reassemble a membrane using entirely different lipids.

Cells produce structurally diverse lipids which serve as the fundamental building blocks of membranes and, hence, play a pivotal role in their survival and functionality (1–4). To adapt to different environments, organisms have evolved diverse mechanisms to modify their so-called lipidome, adjusting the structure and proportions of specific lipids (5, 6). One of the most prevalent forms of membrane lipid adaptation in eukaryotes and most bacteria is the alteration of their ester-linked alkyl chain (fatty acid) composition. Indeed, the carbon chain length, the number and position of unsaturations, and the (methyl) branching patterns of fatty acids significantly impact membrane properties (7). Over the past decades, it has been established that such fatty acid modifications modulate membrane fluidity and permeability as a response to changing conditions including temperature, pH, and hydrostatic pressure (6, 8–10), which has been coined as "homo-viscous adaptation."

In addition to modifying the ester-linked alkyl chain glycerolipids, organisms can also adjust the polar headgroups of their membrane lipids in response to physicochemical or nutrient stress (11–13). For instance, microalgae and cyanobacteria living in the oligotrophic open ocean replace their phospholipids with nonphospholipids such as glycolipids or aminolipids (14). This substitution ensures that phosphorous is used for other essential cellular processes, allowing these organisms to survive in nutrient-limited environments.

Certain eukaryotes and bacteria have developed the ability to synthesize both ether and ester bond alkyl chains, forming mixed ether/ester bond lipids (15–19). In humans, mixed ether/ester bond lipids are found in various organs, including the nervous, immune, and cardiovascular systems, and are commonly referred to as plasmalogens (18). These compounds are characterized by a double bond adjacent to the ether linkage, making them vinyl ether lipids. Plasmalogens play diverse roles in mammalian cellular physiology, including antioxidant defense, membrane structure and dynamics, cell signaling, neural development, and lipid metabolism (20, 21).

In contrast to human tissues, some bacteria synthesize not only plasmalogens, but also mixed ether/ester and diether lipids with various saturated, unsaturated, and branched alkyl chains

Author contributions: S.D., V.G., E.C.H., N.J.B., C.C.-L., and J.S.S.D. designed research; S.D. performed research; V.G., E.C.H., and C.C.-L. contributed new reagents/analytic tools; S.D., E.C.H., and N.J.B. analyzed data; J.S.S.D. supervised the research; and S.D. wrote the paper with contributions from all authors.

The authors declare no competing interest.

This article is a PNAS Direct Submission.

[1]To whom correspondence may be addressed. Email: su.ding@nioz.nl.

[2]Present address: Chemistry Department, Mediterranean Institute of Oceanography (MIO), Aix Marseille Université—CNRS, Marseille 13288, France.

This article contains supporting information online at https://www.pnas.org/lookup/suppl/doi:10.1073/pnas.2400711121/-/DCSupplemental.

Published June 4, 2024.

(16, 22, 23). The synthesis and function of ether lipids in bacteria remain poorly understood, but emerging evidence suggests that their presence may have been at the origin of bacterial adaptation to extreme habitats characterized by high temperatures (24, 25) or extremely low pH (26). It has been hypothesized that ether lipids in bacteria offer higher thermal stability and lower membrane permeability compared to ester lipids. While the presence of bacterial ether and ether/ester bond lipids has mainly been studied in extreme environments, it is important to note that these lipids are widespread in natural environments, such as soils (27), lakes (28), and oceans (24, 29–32), and are synthesized by various non-extremophilic bacteria (19). Hence, exploring the adaptation of bacterial mixed ether/ester bond lipids is critical for understanding the strategies employed by bacteria to thrive in diverse environments.

Only a limited number of studies have conducted comprehensive investigations into lipidomic remodeling across various physicochemical perturbations and nutrient stress (33–37), despite the fact that exploration of the lipidome response to these conditions would offer valuable insight into the molecular mechanisms that govern the functionality of bacterial cellular membranes, probing further the remarkable adaptability and plasticity of biological systems. *Desulfatibacillum alkenivorans* strain PF2803^T (38), a mesophilic sulfate-reducing bacterium, possesses the ability to synthesize a wide array of mixed ether/ester bond lipids (19, 23, 39, 40), which allows the role of this facet of lipidome adaptation to be deciphered. To this end, we characterized its lipidomic adaptivity under varying physicochemical and nutrient conditions including temperature, pH, salinity, and varying concentrations of phosphate [PO_4^{3-}] and ammonium [NH_4^+], respectively (Fig. 1*A*).

Results

An Untargeted Lipidomic Approach Reveals 390 Individual Lipids. *D. alkenivorans* has previously been shown to synthesize diacylglycerols (DAGs), dietherglycerols (DEGs), and "mixed" acyl/ether glycerols [AEGs, containing one ester-bound fatty acid and one ether-bond alkyl chain (19, 39)]. This unusual lipid synthesis capability makes *D. alkenivorans* an excellent model to obtain a holistic picture of lipidome plasticity under variations in temperature, pH, salinity, and nutrient concentration ([PO_4^{3-}] and [NH_4^+]). We employed a previously developed analytical and computational workflow (31, 41) to analyze compositional changes in the lipidome by performing dedicated cultivation experiments in which one of the parameters was varied (Fig. 1; all performed in triplicate to account for natural biological variability). This approach allowed us to systematically collect and analyze high-resolution data-independent MS/MS spectra generated by ultra-high-pressure liquid chromatography coupled with high-resolution tandem mass spectrometry (UHPLC-HRMS^n) analysis of lipid extracts, enabling the thorough deconvolution of the lipidome. By using this untargeted approach (31), 390 individual lipids, belonging to six major classes, were found and putatively identified (Figs. 1*B* and 2*A*). Among these, isoprenoid quinones displayed the highest diversity, with a total of 47 individual species identified. Molecular network analysis (*SI Appendix*, Fig. S1) revealed that only a few menaquinones (MK) were consistently abundant across all culturing conditions, such as MK (8:7), while others were present in trace amounts and showed no significant variation. The remaining five lipid classes were represented by intact polar lipids (IPLs) all composed of 12 to 33 individual lipids (Fig. 2*A*). These latter classes included phosphatidylethanolamines (PE) and phosphatidylglycerols (PG), cardiolipins (CL), and glycolipids with a glucuronosyl (GlcA) headgroup. The core lipids of PE and PG consisted of DAGs, AEGs, and DEGs. GlcA, on the other hand, only contained AEGs (Fig. 3*A*) and DEGs (*SI Appendix*, Fig. S2) as its core lipids. The CL contained four alkyl/acyl chains: tetraetherglycerols (TetraEGs), triether/monoacyl glycerols (TriEGs), diether/diacyl glycerols (DiEGs), monoether/triacyl glycerols (MonoEGs), and tetra-acylglycerols (TetraAGs) (40). In addition, a class of sulfur-containing amino IPLs with a headgroup characterized by a *m/z* 205.064 ($C_7H_{13}O_3N_2S^+$) fragment was observed specifically in the cultures with low [PO_4^{3-}]. Molecular network analysis revealed that these unknown sulfur-containing amino lipids differed from each other by the summed alkyl chain carbon atoms and number of double bonds (Fig. 3*B*). Based on their MS^2 spectra (see for details *SI Appendix*, Figs. S3 and S4 and *Text*), the unknown IPLs are composed of the common core lipids seen in the other IPLs (DAGs, AEGs, or DEGs) bound through glycerol to a polar headgroup (Fig. 3*B* and *SI Appendix*, Figs. S5 and S6) consisting of a butyramide linked to a cysteine moiety. Consequently, we tentatively assigned these sulfur-containing aminolipids as N-butyramide cysteine glycerols (BACys).

Lipidome Modification as a Function of Culture Conditions. To investigate the basis of the lipid adaptation, we performed a detailed analysis of the molecular composition of the lipidome, focusing separately on polar headgroups, alkyl/acyl chains, and ether/ester combinations. The relative abundances of major IPL classes remained relatively stable in response to changes in [NH_4^+], pH and salinity (Fig. 4 *A*–*E*). However, notable changes were observed for the phospholipids when the growth temperature increased from 30 (optimal) to 40 °C. The relative abundances of PG-DEGs and PE-DEGs decreased ($P < 0.01$, Student's *t* tests), while those of PE-AEGs and PE-DAGs slightly increased ($P < 0.01$). Interestingly, the relative abundance of CL significantly increased from 2 to 19% with increasing growth temperature from 30 to 40 °C (Figs. 4*C* and 5*A*). Moreover, significant changes were also observed with the reduction in [PO_4^{3-}]. Under phosphorous starvation, the relative abundance of phospholipids (PG, PE, and CL, Fig. 4 *A*–*C*) decreased significantly from ca. 90% of total lipids to <10%, while that of the nonphospholipids GlcA and BACys showed a prominent increase (Figs. 4 *D* and *E* and 5*A*). Notably, the relative abundance of GlcA rose from <1 to ca. 20% of total lipids, and the newly formed sulfur- and nitrogen-containing lipids, BACys, increased from <1 to ca. 65% of the total lipids as [PO_4^{3-}] was reduced (Fig. 5*A*).

In addition to the changing relative abundance of major lipids with increasing temperature and phosphorus starvation, the number of lipid species also showed marked changes. For example, the number of lipids with a relative abundance >0.5% rose from 18 to 39 when temperature increased from 30 to 40 °C (Fig. 5*B*). This increase is primarily attributed to the significant rise in the number of CL, especially CL-DiEGs and CL-TetraEGs. Additionally, under phosphorus limitation, 21 BACys and 9 GlcA lipid species emerged, each with an abundance >0.5% (Fig. 5*B*). Additionally, at high [PO_4^{3-}], the proportion of P-containing lipids: N-containing lipids: S-containing lipids was approximately 84:15:1. However, under phosphorus limitation, this ratio shifted to 5:63:32. This aligns well with previous studies that showed cyanobacteria can produce 1 to 130-fold increases in sulfoquinovosyldiacylglycerols (SQDG) to substitute PG under phosphorus limitation (14, 42).

A Marked Decline in Phospholipids Abundance upon Phosphorous Stress. To gain a comprehensive view of the overall trend of total diglyceride phospholipids, CL, and non-phospholipids under the culturing conditions, we combined the different types of

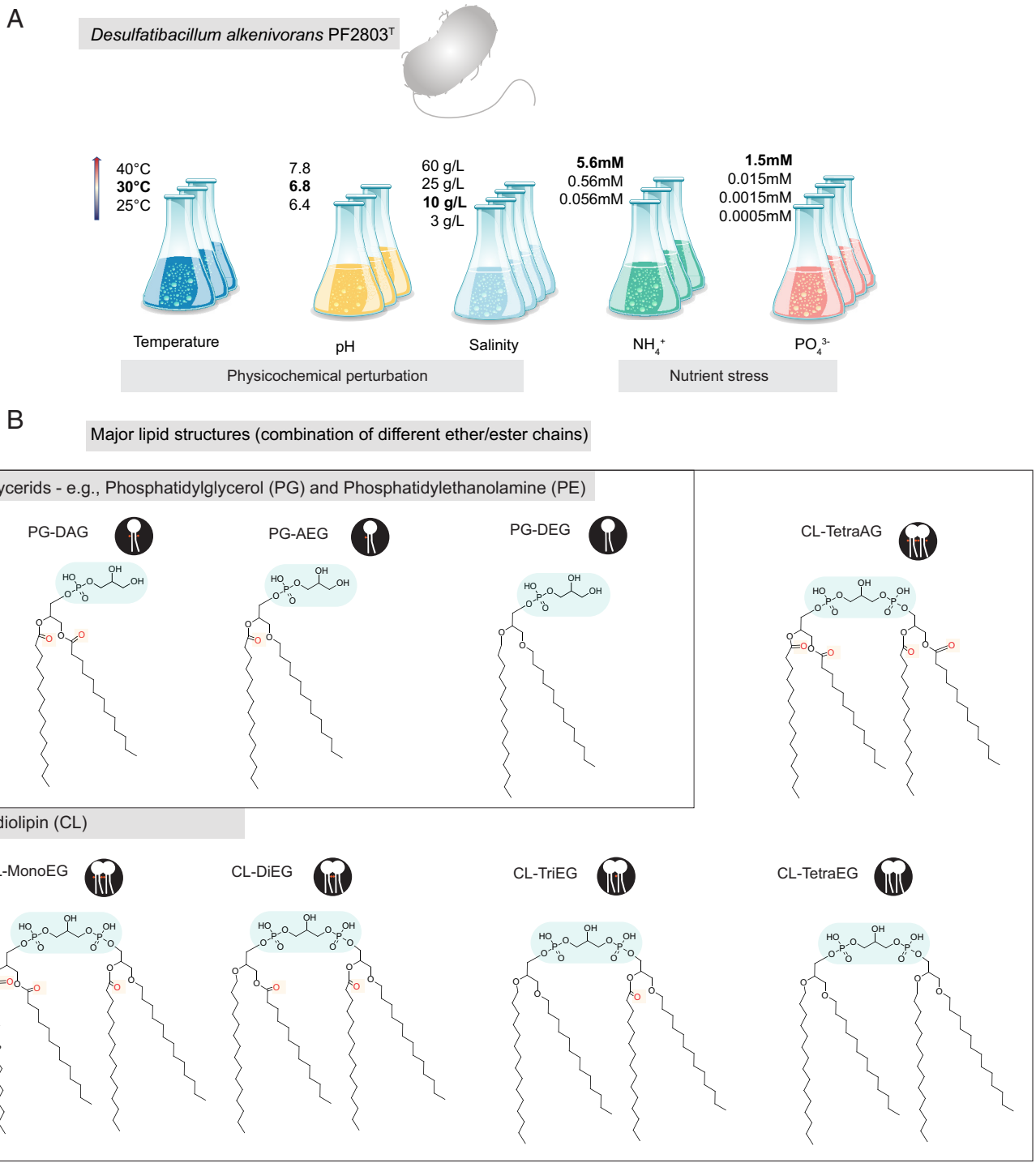

Fig. 1. Overview of the experimental outline and characteristic examples of common lipids in the lipidome of *D. alkenivorans*. (*A*) Schematic experimental set-up with the five parameters varied in the cultivation of *D. alkenivorans* indicated. The number in bold font indicates the optimal condition with the highest growth rate for this parameter as reported previously (19, 38). (*B*) Examples of common IPLs of *D. alkenivorans*, including diglycerids and CL. Characteristic of the lipids of this bacterium is that the glycerol core lipids contain two ether, two ester bond, or an ether and an ester bond (40). The oxygen of an ester bond is colored in red. The light blue area indicates the polar head group. Abbreviations: PG, phosphoglycerol; CL, cardiolipin; DAG, diacylglycerol (both chains are ester-bound fatty acids); AEG, acyl/ether glycerol (one chain is an ester-bound fatty acid while the other chain is an ether-bound alkyl chain); DEG, dietherglycerol (both chains are ether-bound alkyl chains); TetraEG, tetra-ether glycerols; TriEG, triether/monoester glycerols; DiEG, diether/diester glycerols; MonoEG, monoether/triester glycerol; TetraAG, tetraester glycerols. The mass spectral identification of CL with different ether/ester bond alkyl chain combinations is described elsewhere (40).

diglyceride phospholipids, CL, and nonphospholipids, respectively. A significant decrease was observed in the ratio of summed diglyceride phospholipids to summed CL with the elevation in temperature and phosphorous stress (Fig. 6*A*, $P < 0.001$). A significant decrease was observed in the ratios of summed phospholipids (including both diglyceride and CL) against summed nonphospholipids in response to phosphorous stress ($P < 0.001$, Fig. 6*B*).

Double Bonds and Chain Length Affected by Changing Culture Conditions. Next, we examined the impact of the different culturing conditions on the number of carbon atoms and double bond equivalents (DBEs) of the alkyl/acyl chains in the cores of all IPLs (Fig. 6 *D* and *E* and *SI Appendix*, Fig. S7). IPLs with 0 DBEs were by far the most abundant, comprising 92 ± 3% of the total IPLs. The average DBEs of all IPLs were strongly affected by phosphate

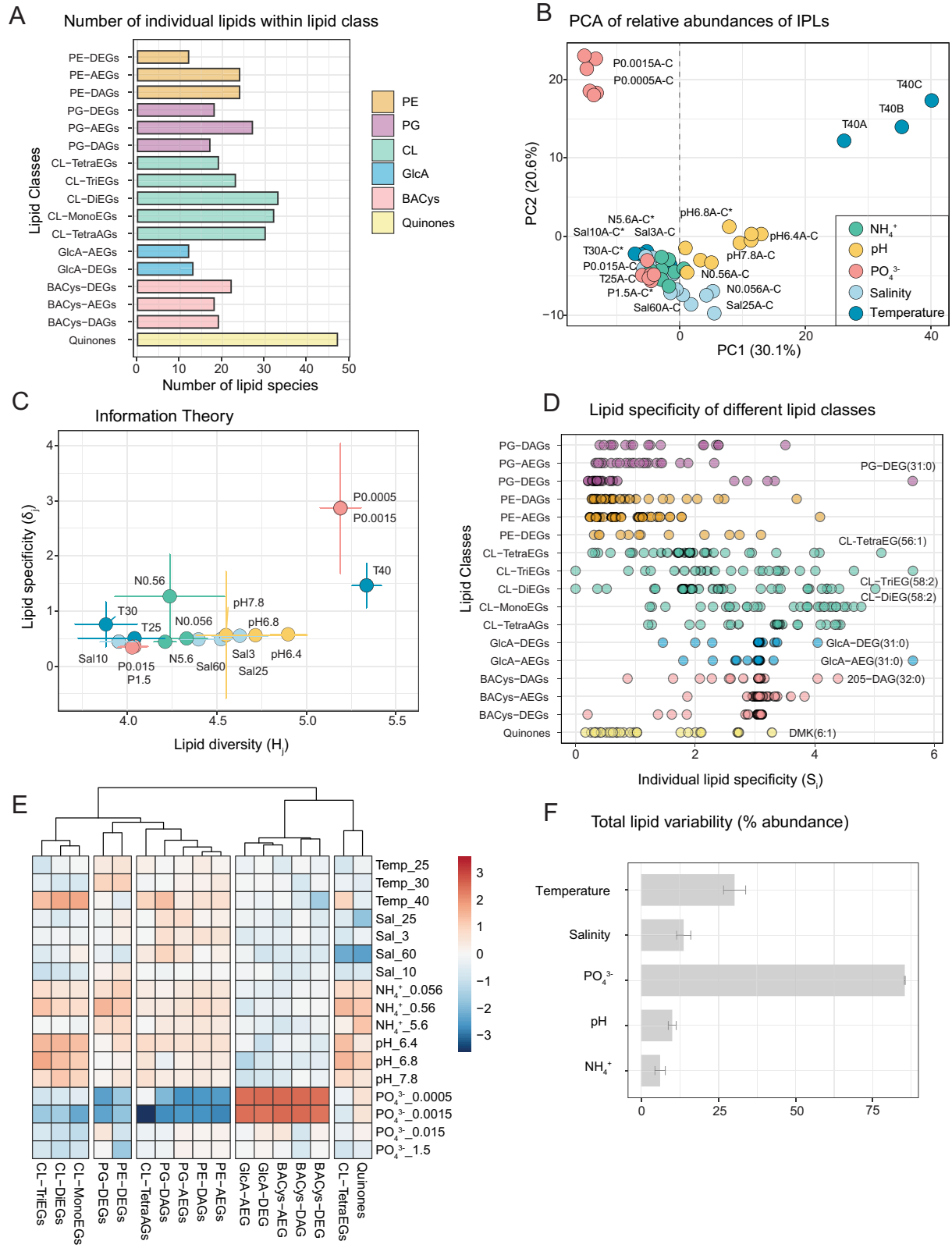

Fig. 2. The impact of culturing conditions on the lipidomic variability of *D. alkenivorans*. (*A*) The number of IPL species in different lipid classes putatively identified in this study. (*B*) PCA using the relative abundances based on peak intensity of IPL species, showcasing the variation in general lipidomic features across individual experimental conditions. (*C*) Information theory analysis applied to the lipidome showing its diversity (H_j index) and specialization (δ_j index) based on the Shannon entropy of the lipidomic frequency distribution. (*D*) The individual lipid species specificity (S_i index) for each lipid class, taking into account all cultivations at different conditions. (*E*) Hierarchical clustering heatmap depicting the distribution of major lipid classes across all the culturing conditions. The color bar on the right side represents the Z-score normalization scale of lipid class abundance, which ranges from −3 to +3 SDs. (*F*) Cumulative variability of all intact polar lipid species within each range of growth conditions, calculated as the difference in mean abundance between the standard growth condition and the variable conditions (33). This variability analysis excludes the data obtained at a [PO_4^{3-}] of 0.015 mM as under these phosphorous-sufficient condition, the lipidome composition was highly comparable to that obtained at the standard growth condition (1.5 mM). Each condition analysis is based on three biological replicates. Note that the color key in (*A*) applies to all panels. Abbreviations: Polar head groups—phosphatidylethanolamines (PE), phosphatidylglycerols (PG), cardiolipins (CL), novel N-butyramide cysteine (BACys), glucuronosyl (GlcA); Core lipids—diacylglycerols (DAGs), acyl/ether glycerols (AEGs), dietherglycerols (DEGs), tetraetherglycerols (TetraEGs), triether/monoacyl glycerols (TriEGs), diether/diacyl glycerol (DiEGs), monoether/triacyl glycerol (MonoEGs), and tetraacylglycerols (TetraAGs), demethylmenaquinone (DMK).

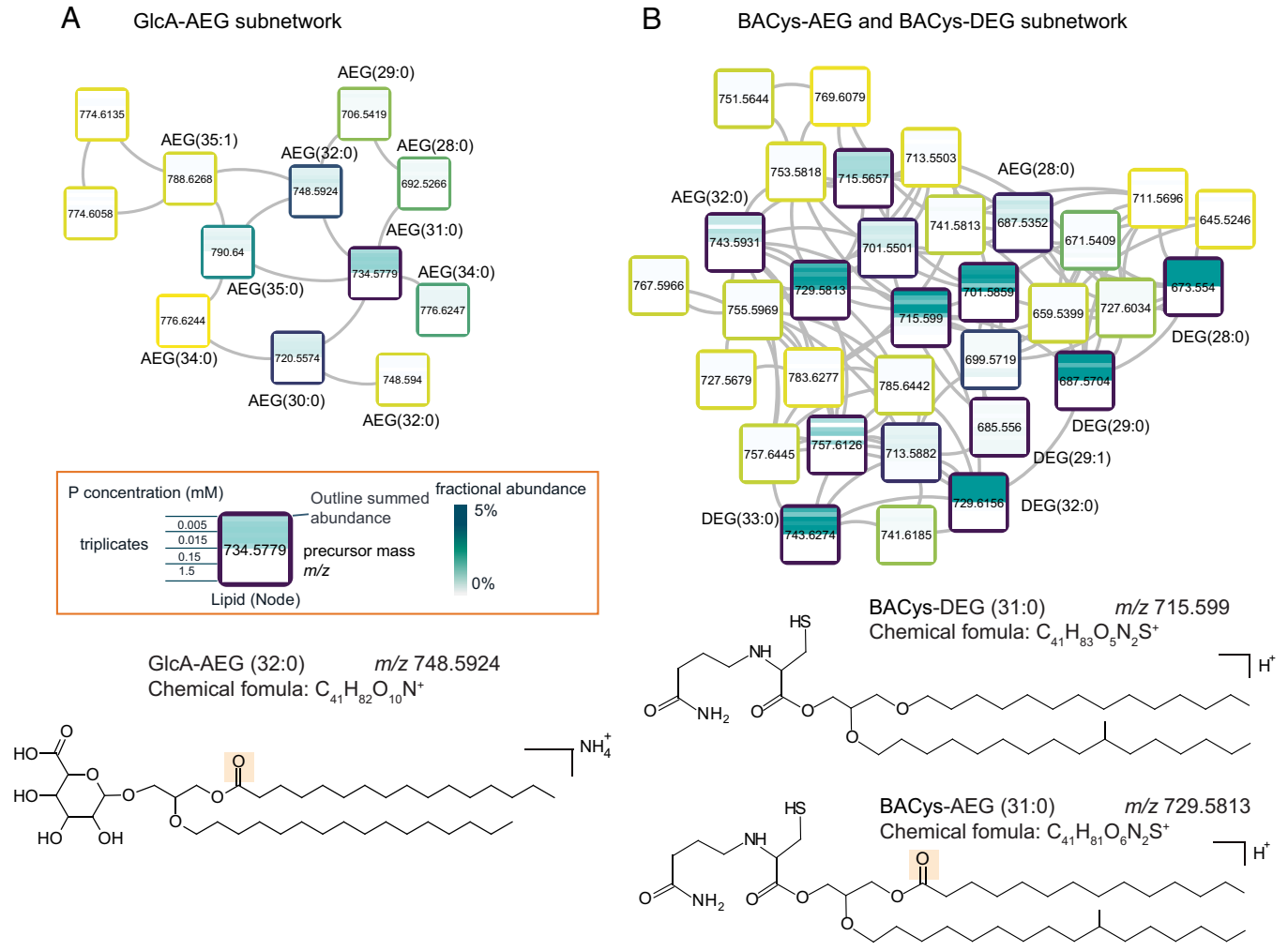

Fig. 3. Subnetworks of GlcA-AEGs and S-containing aminolipids, butyramide cysteine (BACys), with AEGs and DEGs in the lipidome of *D. alkenivorans* in response to different PO_4^{3-} conditions. (*A*) Subnetwork of GlcA-AEGs. (*B*) Subnetwork of BACys-AEGs and BACys-DEGs. Each box within the figure represents a specific lipid species, with the numeric value indicating its precursor mass. Connections between the boxes (representing lipids) indicate that these lipids have a mass spectral similarity cosine greater than 0.6 (see *Materials and Methods* section for details). The heatmap inside each box illustrates the distribution (fractional abundance) of the respective lipid species across the four PO_4^{3-} concentrations used. Each PO_4^{3-} concentration has three bands in the heatmap to show the abundance of the lipids from the triplicate experiments. The color of the box border represents the total abundance of lipid species across all cultured samples; the darker it is, the more abundant the lipid. The heatmap reveals the absence of GlcA and BACys under phosphorous-sufficient conditions (1.5 and 0.015 mM), contrasted by their prominence under phosphorous-limiting conditions (0.0005 and 0.0015 mM). Characteristic examples of the GlcA and BACys structures are shown.

limitation ($P < 0.001$), and to a lesser extent by temperature ($P = 0.004$), pH ($P = 0.009$), and salinity ($P = 0.002$). In contrast, $[NH_4^+]$ did not influence DBEs (Fig. 6*D*). The majority of alkyl/acyl chains contained between 28 and 32 carbon atoms (79 ± 7%) (Fig. 6*E*). Similar to DBEs, the average number of carbon atoms of the alkyl/acyl chains was highly conserved under varying pH and $[NH_4^+]$. However, it exhibited significant variability in response to changes in $[PO_4^{3-}]$ ($P < 0.001$) and, to a lesser extent, salinity ($P = 0.002$), and temperature ($P = 0.015$) (Fig. 6*E*).

Minimal Changes in the Ratio of Ether/Ester Bonds. To determine the role of ether/ester bond changes in lipidome adaptation, we further investigated the major lipid classes with varying ether/ester combinations (Figs. 4 and 6*C*). Within PG, significant changes were observed in those with DEGs as core lipids under $[PO_4^{3-}]$ limitation and temperature elevation but not with AEGs and DAGs (Fig. 4*A*). For PE, a significant decrease was observed in DEGs under decreased $[PO_4^{3-}]$ and temperature elevation, while the relative abundance of AEGs and DAGs increased when temperature was elevated (Fig. 4*B*). Similar trends were also observed in CL with different combinations of ether/ester bonds when facing a temperature increase (Fig. 4*C*). For the non-phospholipids GlcA and BACys, DEGs and AEGs were found to significantly increase at phosphate limitation, but not under other conditions. When we examined the ratio of ether/ester chains among all lipid combined, we found that it was less significant compared to the impact of polar headgroups when temperature was elevated or under $[PO_4^{3-}]$ limitation (Fig. 6*C*, $P < 0.05$). This observation aligns with previous research that utilized a hydrolysis-based method to analyze core lipids of *D. alkenivorans*, where the proportion of alkylglycerol ether lipids was found to remain relatively stable regardless of the growth temperature (39). Furthermore, as we examined the overarching pattern of ester bond lipids versus ether bond lipids, we observed significant shifts from ester bond lipids to ether bond lipids when transitioning from suboptimal to optimal salinity conditions (Fig. 6*C*, $P < 0.001$).

Structural Diversity and Specificity of Lipidome across Culture Conditions. In order to assess the general variation in the lipidome of *D. alkenivorans* strain across all experimental conditions and replicates, we conducted a principal component analysis (PCA) on the abundances of lipid species, based on peak intensity (Fig. 2*B*). The first principal component (PC1) explained 30.1% of the variance of all the lipids and the second principal component (PC2) explained 20.6%. The majority of the applied culture conditions clustered

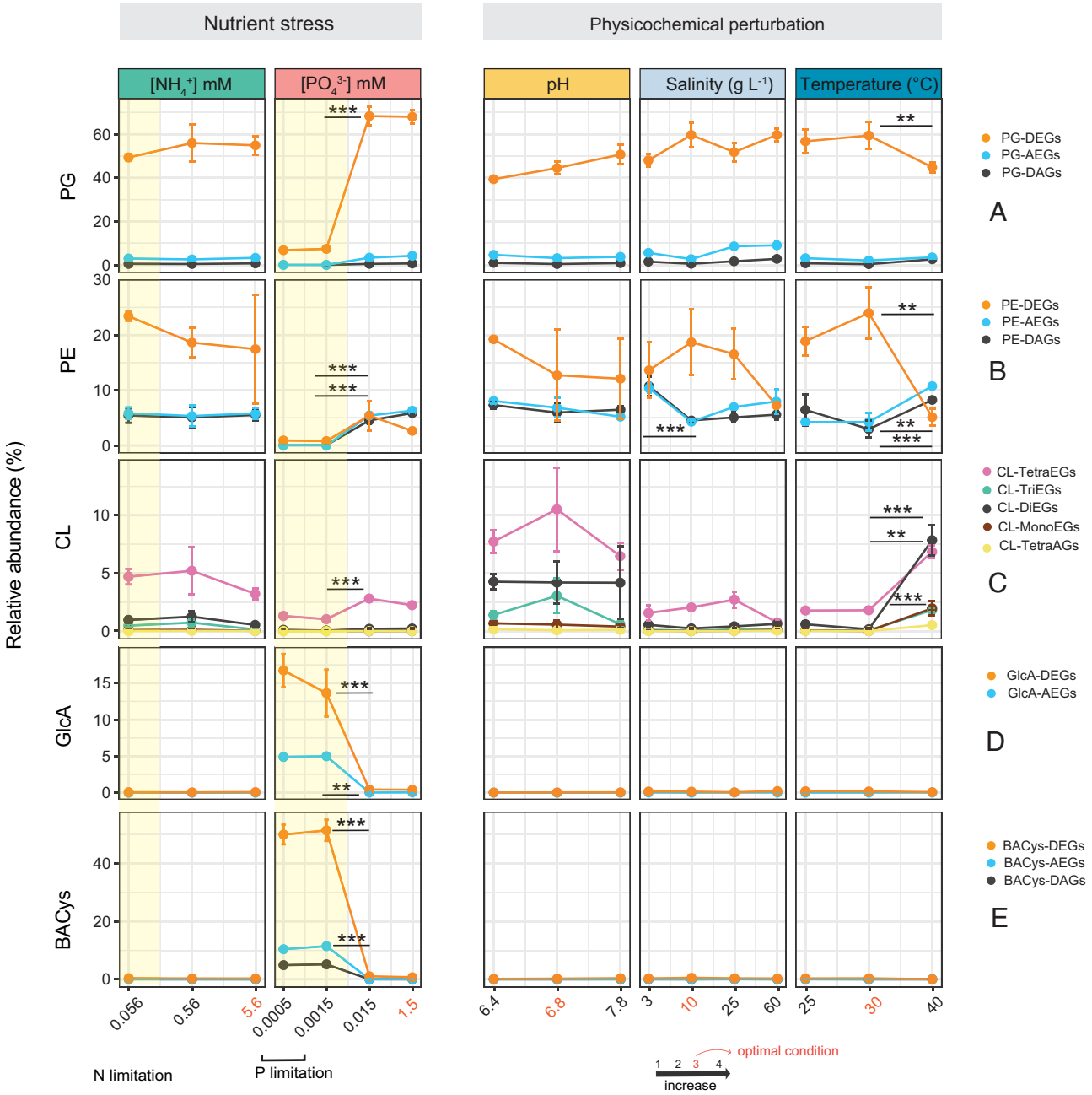

Fig. 4. Variability of major lipid classes in the lipidome of *D. alkenivorans* across different culturing conditions. (*A*) PG with different ether/ester bond core lipids. (*B*) PE with different ether/ester bond core lipids. (*C*) CL with different ether/ester bond core lipids. (*D*) GlcA with different ether/ester bond core lipids. (*E*) Novel BACys with different ether/ester bond core lipids. Asterisks indicate significant differences between the last condition and the current condition (Student's *t* tests on pairwise differences, $*P < 0.05$, $**P < 0.01$, and $***P < 0.001$). The numbers of treatments on the *x*-axis represent the parameters associated with each condition, ranging from low to high. These parameters include temperature (25 °C, 30 °C, 40 °C), pH levels (6.4, 6.8, 7.8), NaCl concentration (3, 10, 25, 60 g L^{-1}), PO_4^{3-} concentration (0.0005, 0.0015, 0.015, 1.5 mM), and NH_4^+ concentration (0.056, 0.56, and 5.6 mM). The optimal conditions for growth are indicated in red font.

closely together, with the exception of the highest temperature (40 °C) and the two lowest [PO_4^{3-}] concentrations (0.0015 and 0.0005 mM). The noticeable separation of the lipidome produced at the highest temperature and the most limiting [PO_4^{3-}] from those biosynthesized at the other culturing conditions illustrates that these two parameters have the most substantial influence on the *D. alkenivorans* lipidome (Fig. 2*B*).

To further evaluate the lipidome plasticity under various physicochemical perturbations and nutrient stress, we applied an information theory framework (43, 44). This framework allowed us to measure both the lipidome diversity (H_j index) and specialization (δ_j index) based on the Shannon entropy of the lipidomic frequency distribution. The lipidome diversity (H_j index) represents the extent of variation in its composition at a specific culturing condition. A high value of the H_j diversity index indicates either a larger proportion of lipids detected or a more evenly distributed abundance of lipids under that condition. The lipidome specialization δ_j index reflects the average degree of uniqueness of individual lipids and is thus an indicator for the average lipid specificity for a particular culturing condition. By cross-plotting the specialization and diversity of the *D. alkenivorans* lipidome, we observed a similar grouping for most culturing conditions, except for those involving the highest temperature employed (40 °C) and the lowest (limiting) [PO_4^{3-}] (1.5 and 0.5 mM; Fig. 2*C*). Interestingly, cultivation under phosphate limitation displayed the second-most diverse lipidome profile and the highest specialization among all

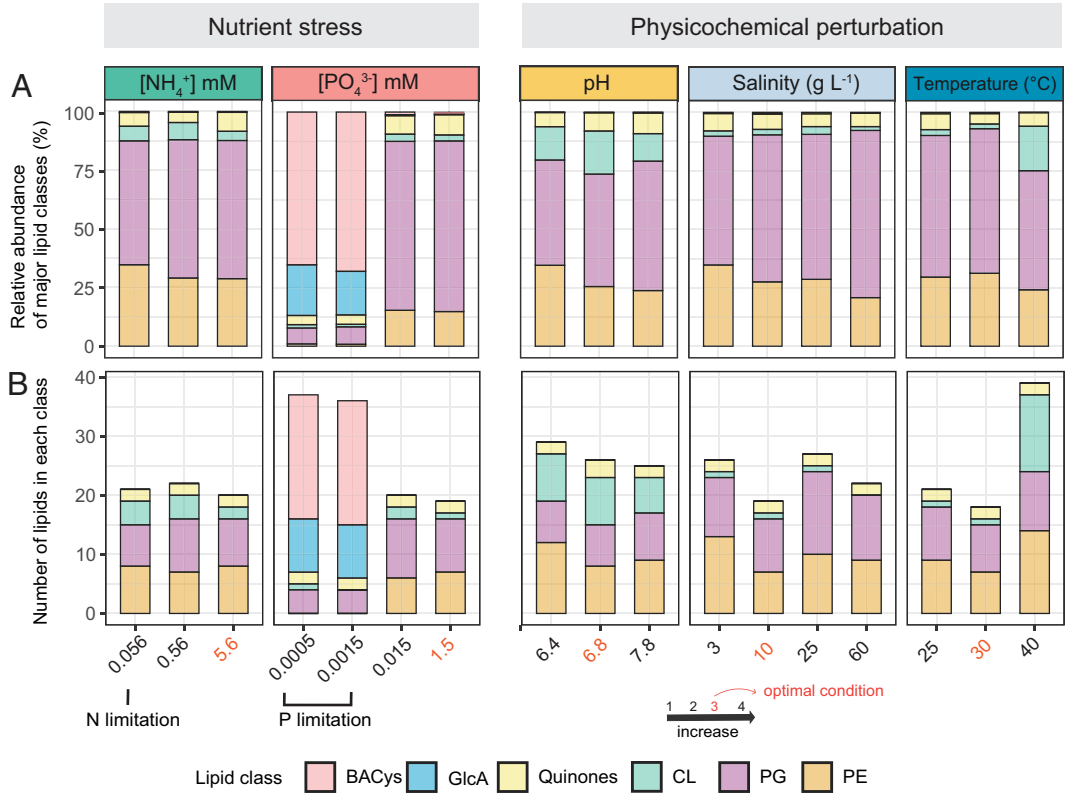

Fig. 5. Distribution of the relative abundance of major lipid classes and number of lipid species in the lipidome of *D. alkenivorans* across different culturing conditions. (*A*) Relative abundance of major lipid classes. (*B*) Number of lipid species with an abundance exceeding 0.5% of the total lipids. The numbers of treatments on the *x*-axis represent the parameters associated with each condition, ranging from low to high. These parameters include temperature (25 °C, 30 °C, 40 °C), pH levels (6.4, 6.8, 7.8), NaCl concentration (3, 10, 25, 60 g L^{-1}), PO_4^{3-} concentration (0.0005, 0.0015, 0.015, 1.5 mM), and NH_4^+ concentration (0.056, 0.56, and 5.6 mM). The optimal conditions for growth are indicated in red font.

cultivation conditions. High growth temperature (40 °C) exhibited the highest diverse lipidome profile of all culture conditions, while still maintaining a relatively high level of specialization, especially when compared to that of 25 and 30 °C. We subsequently calculated the lipid species specificity (S_i index) for all the lipid species across the various culturing conditions (Fig. 2*D*). The S_i specificity index allows us to identify which lipids exhibit the highest degree of specificity or sensitivity toward changes in the culturing conditions. Among the lipid species analyzed, a large number of lipids had small values of S_i ($S_i < 3.0$, 77% of the total), indicating they were either present in low concentrations or uniformly distributed across all the culturing conditions. On the other hand, a few specific lipids, such as PG-DEG (31:0, a summed chain length of 31 carbons with 0 double bond), CL-TetraEG (56:1), CL-TriEG (58:2), GlcA-DEG (31:0), GlcA-AEG (31:0), and BACys-DAG (32:0), demonstrated a higher level of specificity toward particular culturing conditions.

We also applied a hierarchical clustering heatmap to analyze the distribution of major lipid classes across all the culturing conditions of *D. alkenivorans* (Fig. 2*E*). This visualization method allowed to assess the similarity of lipid class profiles and rapidly examine major lipid class changes under different culturing conditions. The major lipid classes were grouped into four distinct clusters. The first cluster consisted of all the nonphospholipids (GlcA and the novel BACys). The second cluster comprised phospholipids, specifically PG and PE. The third cluster included CLs with 1-3 ether chains, while the fourth cluster consisted of CL-TetraEGs and isoprenoid quinones.

In order to assess the impact of perturbations in culturing conditions on the remodeling of the membrane lipidome, we quantified the cumulative variability of all lipid species within each range of growth conditions (Fig. 2*F*). The variability of lipid species was determined by calculating the difference in mean abundance between the optimal growth condition and the sub- and supraoptimal conditions (33). The total lipidomic variability was then obtained by aggregating the absolute value of the changes in abundance for all individual lipid species. Among the range of conditions considered in this study, the availability of phosphate exhibited the most significant effect on lipidome remodeling, accounting for 85% of the total lipidomic variability under P-stress conditions. Additionally, supraoptimal temperature was found to have a substantial impact (~25%), resulting in more than a twofold increase in variability compared to the remaining conditions.

Discussion

To date, there have been limited studies systematically characterizing the lipidomic adaptation of living cells under both physicochemical perturbation and nutrient stressors (33–37). To determine which parameter most significantly influences the lipidome adaptation of *D. alkenivorans*, we utilized molecular network analysis to assess changes in the complete lipidome under various culturing conditions. Our analysis included lipids with diverse combinations of ether/ester bond-alkyl chains. Nearly 400 individual lipid species were putatively identified in *D. alkenivorans*, including novel GlcA and BACys lipids. This extensive lipid profiling allowed us to elucidate how lipid structural features, such as the type of polar headgroup, alkyl/acyl chain saturation, alkyl/acyl chain carbon atom numbers, and the ether/ester bond ratio, contribute to membrane adaptation in *D. alkenivorans*.

Isoprenoid quinones are among the most important membrane lipids found in most bacteria and archaea (45) and also form a substantial part (ca. 4 to 9%) of the lipidome of *D. alkenivorans* (Figs. 2*A*

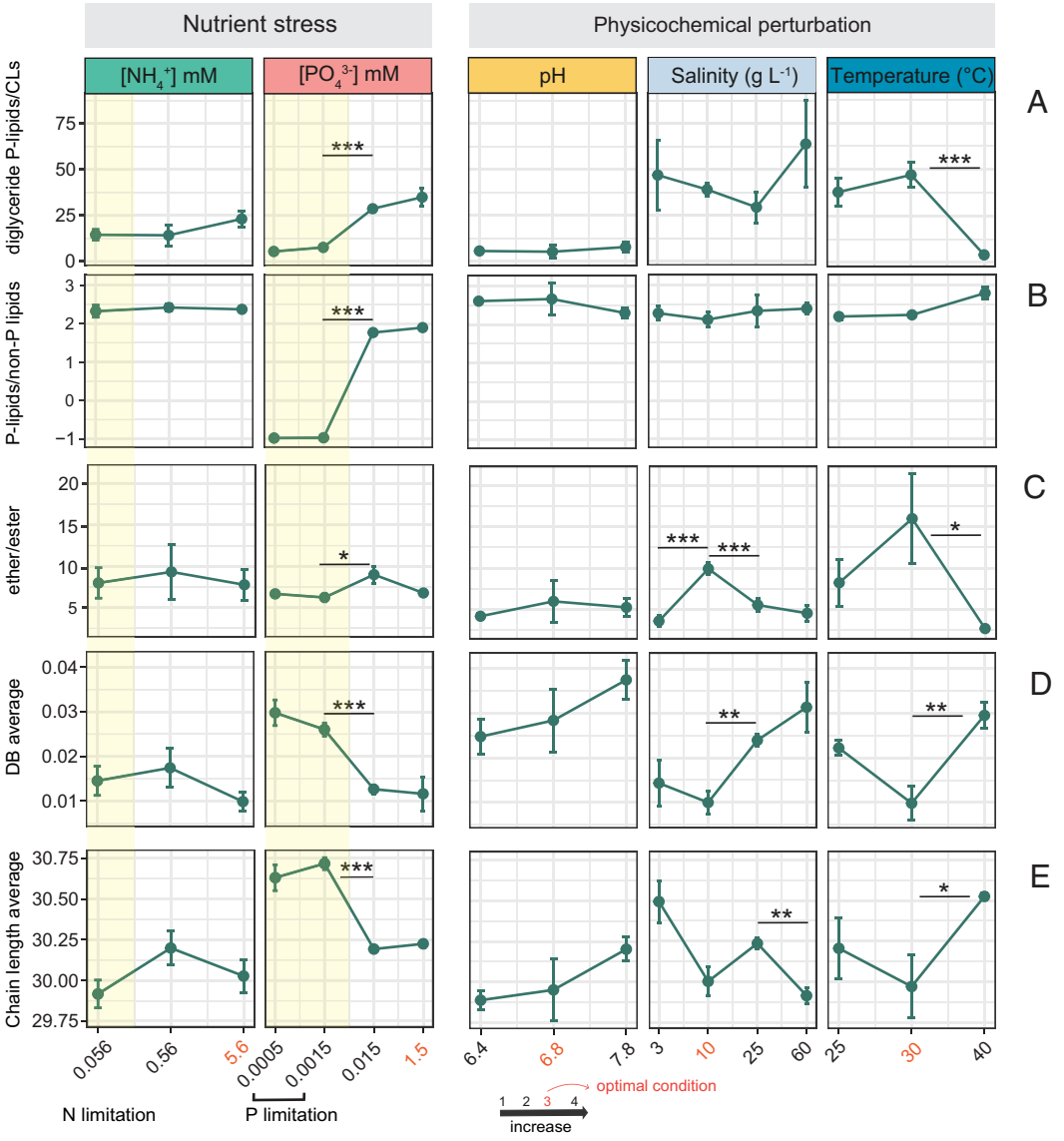

Fig. 6. Adaptation of ether/ester bond lipids, polar headgroups, the averaged carbon chain length, and double bond equivalents (DB) in the lipidome of *D. alkenivorans* across different culturing conditions. (*A*) The ratio of phospholipids with dialkyl chains and tetraalkyl chains, or the ratio of (PE+PG)/CL, calculated as the summed core lipids within each class. (*B*) The logarithmic ratio of phospholipids/nonphospholipids, phospholipids included both diglyceride phospholipids (PG and PE) and CL. (*C*) The ratio of ether/ester bond lipids. The abundance of ethers in lipids with DEGs is calculated based on their inherent intensity, while the abundance of ethers in lipids containing both ether and ester chains is determined using the ratio of ether% multiplied by the intensity. For instance, in CL-TriEG, which has three ether-bond chains and one ester-bond chain, the abundance of the ether chain is calculated as 0.75 multiplied by the intensity. (*D*) The average DBs of total lipids across different culturing conditions. (*E*) The average chain length of two-chain lipids across different culturing conditions. Asterisks indicate significant differences between the last condition and the current condition (Student's *t* tests on pairwise differences, $*P < 0.05$, $**P < 0.01$, and $***P < 0.001$). The numbers of treatments on the *x*-axis represent the parameters associated with each condition, ranging from low to high. These parameters include temperature (25 °C, 30 °C, 40 °C), pH levels (6.4, 6.8, 7.8), NaCl concentration (3, 10, 25, 60 g L^{-1}), PO_4^{3-} concentration (0.0005, 0.0015, 0.015, 1.5 mM, and NH_4^+ concentration (0.056, 0.56, and 5.6 mM). The optimal conditions for growth are indicated in red font.

and 5). They primarily function as electron and proton carriers within photosynthetic and respiratory electron transport chains (45). We did not observe significant changes in the distribution of the isoprenoid quinones under the widely changing conditions of cultivation (Fig. 5 and *SI Appendix*, Fig. S1). This observation supports that isoprenoid quinones reflect the metabolic type of the organism rather than contributing to membrane adaptation (46). However, our findings highlight the effects of the altering culturing conditions on the adaptation of membrane lipidome (IPLs) of *D. alkenivorans* with a dominant role of temperature and $[PO_4^{3-}]$.

Influence of Temperature on the Lipidome Remodeling. Increasing temperature leads to a higher diversity of lipids in *D. alkenivorans*, exemplified by the increased relative abundance of CL (Fig. 4*C*); they increased from 2 to 20% of total lipids when temperature was increased from 30 to 40 °C (Fig. 4*C*). In addition, a markedly increased number of individual CL species with different ether/ester chain combinations was noted at 40 °C (Fig. 5*B*). The particularly anionic CL have been proposed to be beneficial in interactions with divalent cations (47, 48). For example, under elevated Mg^{2+} concentrations, the negatively charged CL lipid assists cells in counteracting curvature stress and protects the cell's interior from an elevated level of toxic Na^+ (35), but salinity had no large effect On the CL abundance and composition (Fig. 5). CL may also play a compensatory role by counteracting the effects of enhanced phospholipid saturation and is essential for cristae development in environments with low oxygen levels (49). Under high temperature, it is possible

that the upregulation in CL production may have assisted *D. alkenivorans* control curvature stress and optimally balance membrane permeability. The finding of a dominant effect of temperature on lipidome remodeling is similar to that observed in *Methylobacterium extorquens* (33), suggesting a commonality in lipidome adaptation between these two diverse bacteria.

Previous studies have shown that increasing the number of DBEs per lipid increases lipid mobility and hence counteracts low temperature-induced membrane rigidity (8, 50). In this study, we did not observe a clear relationship between DBEs and growth temperature (Fig. 6). In fact, the lipidome has a highly "saturated" nature (Fig. 6*D*; DBE average always below 0.04), fully in line with previous work on its core lipid composition (39). Similarly, dominant saturated lipids have also been detected in cultured bacteria from the order *Rubrobacterales* (16) and *Thermodesulfobacteriales* (51). This characteristic may serve as a common feature for the membrane lipid building blocks of anaerobic bacteria. Interestingly, IPLs that are highly saturated, particularly DEGs with 0 to 1 DBEs, predominate in deep waters of the euxinic Black Sea (31) and the oxygen minimum zone of the eastern tropical North Pacific Ocean (30).

The chain length adaptation of bacterial core lipids has also been reported at elevated temperatures (8). However, similar to DBEs, a minimal influence of temperature on lipid chain length of IPLs was observed in *D. alkenivorans* (Fig. 6*E*). A study evaluating the impact of temperature on the hydrolyzed core lipid composition of sulfate-reducing bacteria including *D. alkenivorans, Desulfatibacillum aliphaticivorans, and Thermodesulfobacterium commune* also indicated a minimal influence of temperature on lipid chain length (39). The potential influence of other parameters, such as pressure, on chain length and DBE remodels still requires further investigation.

The thermal stability of ether bonds compared to ester bonds, along with the frequent occurrence of nonisoprenoid ether glycerol lipids in thermophilic bacterial strains, has often been regarded as another adaptation to withstand high temperatures (5). For instance, *Acididesulfobacillus,* which thrives in extreme conditions at temperatures exceeding 80 °C, contains significant amounts of ether lipids (52, 53). However, the production of ether lipids is not limited to thermophilic bacteria (19, 37, 54), and not all thermophilic bacteria synthesize ether lipids (17). In an analysis of the core lipid (ether/ester) content of two mesophilic (*D. alkenivorans* and its close relative *D. aliphaticivorans*) and one thermophilic (*T. commune*) sulfate-reducing bacteria, Vinçon-Laugier et al. (39) observed that the ether/ester lipid content remained remarkably stable regardless of the growth temperature. The major adaptive mechanisms involved modifications in the degree and position of methyl branching within the lipid chains. The present study of the complete intact lipidome of *D. alkenivorans* confirms that the ratio of summed ether/ester lipid content remains stable with temperature changes (Fig. 6*C*). However, significant changes in the ether/ester lipid content were observed within a specific lipid class, i.e., CL. CL with more ether chains, such as CL-TetraEGs and CL-DiEGs, increased from less than 2 to ~7% of the total lipids when the temperature was increased from 30 to 40 °C (Fig. 4*C*). In contrast, CL with four ester chains, CL-TetraAGs, remained relatively stable (<0.5%). This suggests that the adaptation of ether/ester chains has occurred in specific lipid classes to help maintain membrane integrity and functionality. Again, this is in line with previous findings on membrane adaptation of *M. extorquens*, which showed headgroup-specific effects of acyl chain variability on its membrane properties (33).

Influence of [PO_4^{3-}]on the Lipidome Remodeling. When subjected to [PO_4^{3-}] limitation, *D. alkenivorans* demonstrates a remarkable metabolic shift characterized by the almost complete replacement of the phospholipids PE, PG, and CL into nonphospholipids, BACys and GlcA (Fig. 5). This adaptive response leads to an increase of both diversity and specificity of the lipidome (Fig. 2). Apparently, *D. alkenivorans* possesses a remarkable genetic capacity to switch to a completely new set of membrane lipids at times of phosphate scarcity.

Previous research has indicated that certain bacteria, when grown under phosphorous-limited conditions, synthesize nonphospholipids such as betaine lipids (55, 56), ornithine lipids (57, 58), and glycolipids (13, 58) and use them as membrane lipids. The presence of the GlcA polar headgroup, as observed in this study, has also been reported in the free-living marine bacteria of the order *Pelagibacterales* (SAR11) (13), in microalgae (59) and in higher plants (60), facing phosphorus starvation. The notable difference observed here lies in the ability of *D. alkenivorans* to incorporate GlcA with various core lipids, ranging from DAGs to AEGs and DEGs. Additionally, this study reports the identification of BACys lipids in bacteria, serving as functional lipids under phosphorus stress. A "sulfur-for-phosphorus" strategy was reported earlier for picocyanobacteria which synthesize SQDG (14, 42), membrane lipids that contain sulfur and sugar, to replace phospholipids in phosphorous-deprived environments. The polar headgroup of BACys lipids distinguishes itself from those of the GlcA and SQDG lipids, in the fact that they are sulfur-containing aminolipids. This indicates that microorganisms can respond to environmental phosphorus shortages through diverse combinations of polar head groups rather than by relying solely on fixed types of non-phospholipids. A class of sulfur-containing aminolipids was found to occur widespread in marine *roseobacters* (61). These lipids, which have been confirmed as cysteinolides recently (62), play a crucial role in biofilm formation by these bacteria. However, whether they have an impact on adaptation to phosphorus limitation still requires further investigation.

Homeoviscous Fine-Tuning of the Lipidome. When facing elevated temperature or [PO_4^{3-}] limitation, the homeoviscous adaptation of *D. alkenivorans* is not an isolated event that focuses exclusively on the polar headgroups. Our study indicates that "homoviscous adaptation" in *D. alkenivorans* is finely tuned through the coordinated regulation of polar headgroup composition, the ratio of ether/ester bonds within specific lipid classes, and the degree and position of methyl branching of the alkyl and acyl chains (38), with a much less dominant role for the adjustment of the alkyl/acyl chain length and DBEs. Rather than just individual changes in one factor, the intricate interplay between different lipid characteristics in achieving optimal adaptive responses of the lipidome seems to be the key.

The exploration of how microbes perceive changes in their biophysical characteristics and adapt through lipidome remodeling has gained significant attention (33). Understanding the underlying mechanisms of membrane lipids' responsiveness would answer a fundamental question regarding the essential requirements for a system to demonstrate lifelike adaptability. Moreover, it could offer valuable insights for designing synthetic membranes from scratch, serving as a blueprint for future engineering endeavors. Our study provides valuable insights into the molecular mechanisms of ether/ester bond lipids, encompassing various polar headgroups that play a crucial role in the functionality of cellular membranes. By examining these lipid compositions, we gain a deeper understanding of the intricate processes that govern membrane stability and function in sulfate-reducing bacteria. Delving deeper into the mechanisms of the ether/ester bond lipid producers holds the potential to uncover the intricate interplay between membrane lipid structure and function.

Materials and Methods

Cultures. *D. alkenivorans* PF2803^T is a mesophilic bacterium belonging to the family *Desulfatibacillaceae* and is known for its ability to degrade *n*-alkenes (39). It was isolated from oil-polluted sediments in Fos Harbour, France (38). For cultivation, *D. alkenivorans* was grown on synthetic sulfate-reducing medium supplemented with octanoate (>99%, Sigma-Aldrich) as the sole carbon and energy source. Cultures (100 mL) were performed in batches for different conditions and were incubated under anaerobic conditions without shaking. The optimal conditions for growth are temperature 30 °C, pH 6.8, [NaCl] 10 g L^{-1}, [PO_4^{3-}] 1.5 mM, and [NH_4^+] 5.6 mM. KH_2PO_4 and NH_4Cl were added to the culture medium to reach the different concentrations for phosphorus and nitrogen. To investigate the effects of different parameters on the lipidome adaptation of *D. alkenivorans*, triplicate cultures were established by varying one parameter affecting growth, while the other parameters remained at their optimal values. These variations in growth parameters applied were temperature (25, 30, and 40 °C), pH (6.4, 6.8, and 7.8), and NaCl concentration (3, 10, 25, and 60 g L^{-1}), PO_4^{3-} (0.0005, 0.0015, 0.015, and 1.5 mM), and NH_4^+ (0.056, 0.56, and 5.6 mM) concentrations. The cultures were incubated for a period of 1 to 3 wk, and growth was monitored for each condition by measuring the optical density to ensure that all cultures reached the end of the exponential phase before collection (Dataset S2). The optical density varied between 0.1 and 0.3 according to different culturing conditions, corresponding to approximately 2.5 to 10 × 10^7 cells/mL, respectively (Dataset S2). The cultures were subsequently filtered on glass microfiber filters (GF/F; Whatman) and stored at −80 °C until extraction of their lipidome.

Lipid Extraction and Analysis. A detailed description of lipid extraction and measurement can be found in ref. 41. Briefly, the filtered cells were extracted using a modified Bligh–Dyer extraction method (51). Medium blanks and extraction blanks were used to subtract background compounds and contaminants. The samples and blanks were extracted ultrasonically for 10 min, twice in a mixture of methanol, dichloromethane (DCM), and PO_4^{3-} buffer (2:1:0.8, v/v/v) and twice with a mixture of methanol, DCM, and aqueous trichloroacetic acid solution pH 3 (2:1:0.8, v/v/v). The organic phase was separated by adding more DCM and buffer to achieve a final solvent ratio of 1:1:0.9 (v/v/v). This organic phase was then subjected to three more extractions using DCM and dried using a stream of N_2 gas. The resulting extract was reconstituted using a mixture of methanol and DCM (in a ratio of 9:1, v/v) and filtered through 0.45 μm regenerated cellulose syringe filters (4 mm diameter; Grace Alltech). The filtered extracts were subsequently analyzed using an Agilent 1290 Infinity I UHPLC system coupled to a Q Exactive Orbitrap MS (Thermo Fisher Scientific, Waltham, MA). The generated output data files from the ultra-high-pressure liquid chromatography coupled with high-resolution tandem mass spectrometry (UHPLC-HRMS^2) analyses were further processed using MZmine software (63) to extract MS^1 and MS^2 spectra as well as quantify peaks. This processing involved several steps, such as mass peak detection, chromatogram building, deconvolution, isotope grouping, feature alignment, and gap filling (https://ccms-ucsd.github.io/GNPSDocumentation).

Molecular Networking. The MS/MS spectra dataset was analyzed using the Feature-Based Molecular Networking tool available on the Global Natural Product Social Molecular Networking (GNPS) platform (64, 65). MS2LDA (66), MolnetenHance r (67), SIRIUS 5 (68), and Spec2Vec (69) were used to assist the searching and identification of lipids. Molecular networking is a data analysis methodology utilized in untargeted metabolomics studies based on MS/MS analysis. It organizes MS/MS spectra into a network-like map, where molecules with similar spectral patterns are grouped together, indicating their structural similarity. Vector similarities were calculated by comparing pairs of spectra based on at least six matching fragment ions (peaks). This comparison takes into account the relative intensities of the fragment ions as well as the difference in precursor *m/z* values between the spectra (65, 70). The resulting molecular network is generated using MATLAB scripts, where each spectrum is allowed to connect to its top K scoring matches (typically up to 10 connections per node). Edges between spectra are retained if they are among the top K matches for both spectra and if the vector similarity score, represented as a cosine value, exceeds a user-defined threshold. In this study, a cosine value of 0.6 was used, with a cosine value of 1.0 indicating identical spectra.

In cases where an ion component exhibited both $[M+H]^+$ and $[M+NH_4]^+$ ions, the abundance of the component was calculated as the sum of the abundances of both ions. A minimum of six shared fragment ions was required between pairs of related MS/MS spectra for them to be connected by an edge in the molecular network. Each node in the network was connected to a maximum of 10 analogs. In addition, consensus spectra were searched against the GNPS spectral library, allowing for a maximum analog mass difference of *m/z* 500. Maximum size of nodes allowed in a single connected subnetwork was 100. In cases where a significant number of related lipids were present in the dataset (greater than 100), they were separated into different subnetworks.

The resulting molecular networks were visualized using Cytoscape version 3.9.1 (71, 72). It is important to note that since many of the lipids detected in this study have not been previously described, authentic standards for absolute quantification were unavailable. The lipids were corrected for sample recovery with a 1,2-dipalmitoyl-sn-glycero-3-O-4′-[N,N,N-trimethyl(d9)]-homoserine (DGTS-d9) internal standard and then examined based on their calibrated peak area responses. A threshold of peak intensity of 1 × 10^6 was used to filter out lipids with an abundance below 0.01 mol% of total lipids. Consequently, the relative peak areas do not necessarily indicate the actual relative abundance of different lipids. Nevertheless, this method allowed comparison between different cultivation conditions (73).

Given our extraction and analytical methods, and relying on the annotation provided by the GNPS library and putatively identified by ourselves, it is anticipated that the majority of ion components within the molecular network are lipids. Therefore, the term "lipidome" was used in relevant parts of the discussion where ion components were addressed.

Statistical Analysis. For PCA (Fig. 2*B*), the abundance data of lipid species were initially transformed using the Hellinger distance method (74) to mitigate bias arising from 0 values. These data were then processed and visualized using R software, version 4.1.2. Hierarchical clustering (Fig. 2*E*) was performed using the "ggplot2" and "pheatmap" packages in R, version 4.3.2.

Information Theory framework. Information theory framework (Fig. 2 *C* and *D*) was used to define lipidome diversity and specialization and individual lipid species specificity (43, 44, 75). Lipids were characterized by their own unique MS/MS spectrum and relative frequency of occurrence among all the culturing samples. Lipidome diversity, the H_j index, was calculated using Shannon entropy of MS/MS (lipid species) frequency distribution derived from the abundance of MS/MS precursors by the following equation

$$H_j = -\sum_{i=1}^{m} P_{ij}\log_2(P_{ij}),$$

where P_{ij} correspond to relative frequency of the *i*th MS/MS ($i = 1, 2, \ldots, m$) in the *j*th sample ($j = 1, 2, \ldots, t$), to illustrate how abundant a specific MS/MS spectrum is relative to all others.

The average frequency of the *i*th MS/MS among samples was calculated as

$$P_i = \frac{1}{t}\sum_{j=1}^{m} P_{ij}.$$

Individual lipid species specificity, the S_i index, was defined as the identity of a given MS/MS regarding frequencies among all the samples. The lipid species specificity was calculated as

$$S_i = \frac{1}{t}\left(\sum_{j=1}^{t}\frac{P_{ij}}{P_i}\log_2\frac{P_{ij}}{P_i}\right).$$

Individual lipid species specificity of specific sample was defined as S_{ij} index.

$$S_{ij} = \sum_{j=1}^{t}\frac{P_{ij}}{P_i}\log_2\frac{P_{ij}}{P_i}.$$

The lipidome specialization δ_j index was measured for each *j*th sample, the average of the MS/MS specificities using the following formula

$$\delta_j = \sum_{i=1}^{m} P_{ij}S_i.$$

Data, Materials, and Software Availability. The processed data (.mgf and .csv) with the molecular network and detailed parameter settings can be accessed at GNPS platform (76). All raw (.raw) and centroided (.mzML) mass spectrometry data are available through the MassIVE repository (77). The source data for the figures are provided in the extended dataset in our data repository on zenodo (78). All custom scripts and workflows used to generate data can be found in our data repository on zenodo (78).

ACKNOWLEDGMENTS. We thank M. Koenen for the lipid extraction and I. Mitteau for help with culturing. We acknowledge A. Mets, D. Dorhout, and M. Verweij for technical support and three anonymous referees for their helpful comments on an earlier draft of this manuscript. J.S.S.D. received funding from the European Research Council (ERC) under the European Union's Horizon 2020 research and innovation program (grant agreement no. 694569–MICROLIPIDS) and from a Spinoza award from NWO. V.G. received funding from the French National Research Agency (ANR-12-BSV7-0003) through the project BAGEL (BActerial production of Glycerol Ether Lipids).

Author affiliations: [a]Department of Marine Microbiology and Biogeochemistry, NIOZ Royal Netherlands Institute for Sea Research, Texel SZ 1797, The Netherlands; [b]Laboratoire de Géologie de Lyon: Terre, Planètes, Environnement, CNRS, Université Claude Bernard Lyon 1, Villeurbanne 69622, France; [c]Institut des Sciences Analytiques et de Physico-chimie pour l'environnement et les Matériaux, Universite de Pau et des Pays de l'Adour, CNRS, Pau 64000, France; and [d]Department of Earth Sciences, Faculty of Geosciences, Utrecht University, Utrecht, CB 3584, The Netherlands

1. B. Brügger, Lipidomics: Analysis of the lipid composition of cells and subcellular organelles by electrospray ionization mass spectrometry. *Annu. Rev. Biochem.* **83**, 79–98 (2014).
2. Y.-M. Zhang, C. O. Rock, Membrane lipid homeostasis in bacteria. *Nat. Rev. Microbiol.* **6**, 222–233 (2008).
3. R. E. Summons, P. V. Welander, D. A. Gold, Lipid biomarkers: Molecular tools for illuminating the history of microbial life. *Nat. Rev. Microbiol.* **20**, 174–185 (2022), 10.1038/s41579-021-00636-2.
4. D. E. G. Briggs, R. E. Summons, Ancient biomolecules: Their origins, fossilization, and role in revealing the history of life. *Bioessays* **36**, 482–490 (2014).
5. Y. Koga, Thermal adaptation of the archaeal and bacterial lipid membranes. *Archaea* **2012**, 789652 (2012).
6. R. Ernst, C. S. Ejsing, B. Antonny, Homeoviscous adaptation and the regulation of membrane lipids. *J. Mol. Biol.* **428**, 4776–4791 (2016).
7. K. R. Levental *et al.*, Lipidomic and biophysical homeostasis of mammalian membranes counteracts dietary lipid perturbations to maintain cellular fitness. *Nat. Commun.* **11**, 1339 (2020).
8. M. F. Siliakus, J. van der Oost, S. W. M. Kengen, Adaptations of archaeal and bacterial membranes to variations in temperature, pH and pressure. *Extremophiles* **21**, 651–670 (2017).
9. J. R. Hazel, E. Eugene Williams, The role of alterations in membrane lipid composition in enabling physiological adaptation of organisms to their physical environment. *Progress Lipid Res.* **29**, 167–227 (1990).
10. C. H. Henry *et al.*, Global ocean lipidomes show a universal relationship between temperature and lipid unsaturation. *Science* **376**, 1487–1491 (2022).
11. F. Schubotz, "Membrane homeostasis upon nutrient (C, N, P) Limitation" in *Biogenesis of Fatty Acids, Lipids and Membranes*, O. Geiger, Ed. (Springer International Publishing, Cham, 2019), pp. 823–847.
12. M. Sebastián *et al.*, Lipid remodelling is a widespread strategy in marine heterotrophic bacteria upon phosphorus deficiency. *ISME J.* **10**, 968–978 (2016).
13. P. Carini *et al.*, SAR11 lipid renovation in response to phosphate starvation. *Proc. Natl. Acad. Sci. U.S.A.* **112**, 7767–7772 (2015).
14. B. A. S. Van Mooy *et al.*, Phytoplankton in the ocean use non-phosphorus lipids in response to phosphorus scarcity. *Nature* **458**, 69–72 (2009).
15. D. X. Sahonero-Canavesi *et al.*, Disentangling the lipid divide: Identification of key enzymes for the biosynthesis of membrane-spanning and ether lipids in bacteria. *Sci. Adv.* **8**, eabq8652 (2022).
16. J. S. Sinninghe Damsté *et al.*, Dominance of mixed ether/ester, intact polar membrane lipids in five species of the order *Rubrobacterales*: Another group of bacteria not obeying the "lipid divide". *Syst. Appl. Microbiol.* **46**, 126404 (2023).
17. J. S. Sinninghe Damsté *et al.*, Structural characterization of diabolic acid-based tetraester, tetraether and mixed ether/ester, membrane-spanning lipids of bacteria from the order *Thermotogales*. *Arch. Microbiol.* **188**, 629–641 (2007).
18. H. Goldfine, The appearance, disappearance and reappearance of plasmalogens in evolution. *Progress Lipid Res.* **49**, 493–498 (2010).
19. V. Grossi *et al.*, Mono- and dialkyl glycerol ether lipids in anaerobic bacteria: Biosynthetic insights from the mesophilic sulfate reducer *Desulfatibacillum alkenivorans* PF2803^{T}. *Appl. Environ. Microbiol.* **81**, 3157 (2015).
20. J. M. Dean, I. J. Lodhi, Structural and functional roles of ether lipids. *Protein Cell* **9**, 196–206 (2018).
21. N. Nagan, R. A. Zoeller, Plasmalogens: Biosynthesis and functions. *Progress Lipid Res.* **40**, 199–229 (2001).
22. R. D. Pancost, I. Bouloubassi, G. Aloisi, J. S. Sinninghe Damsté; the Medinaut Shipboard Scientific Party, Three series of non-isoprenoidal dialkyl glycerol diethers in cold-seep carbonate crusts. *Org. Geochem.* **32**, 695–707 (2001).
23. A. Vinçon-Laugier, V. Grossi, M. Pacton, G. Escarguel, C. Cravo-Laureau, The alkyl glycerol ether lipid composition of heterotrophic sulfate reducing bacteria strongly depends on growth substrate. *Org. Geochem.* **98**, 141–154 (2016).
24. E. Flores *et al.*, Bacterial and eukaryotic intact polar lipids point to in situ production as a key source of labile organic matter in hadal surface sediment of the Atacama Trench. *Biogeosciences* **19**, 1395–1420 (2022).
25. D. X. Sahonero-Canavesi *et al.*, Changes in the distribution of membrane lipids during growth of *Thermotoga maritima* at different temperatures: Indications for the potential mechanism of biosynthesis of ether-bound diabolic acid (membrane-spanning) lipids. *Appl. Environ. Microbiol.* **88**, e0176321 (2022).
26. I. Sánchez-Andrea *et al.*, Acetate degradation at low pH by the moderately acidophilic sulfate reducer *Acididesulfobacillus acetoxydans* gen. nov. sp. nov. *Front. Microbiol.* **13**, 816605 (2022).
27. S. Ding *et al.*, Characteristics and origin of intact polar lipids in soil organic matter. *Soil Biol. Biochem.* **151**, 108045 (2020).
28. T. F. Ertefai *et al.*, Vertical distribution of microbial lipids and functional genes in chemically distinct layers of a highly polluted meromictic lake. *Org. Geochem.* **39**, 1572–1588 (2008).
29. S. G. Wakeham *et al.*, Biomarkers, chemistry and microbiology show chemoautotrophy in a multilayer chemocline in the Cariaco Basin. *Deep Sea Res. Part I: Oceanogr. Res. Papers* **63**, 133–156 (2012).
30. F. Schubotz, S. Xie, J. S. Lipp, K. U. Hinrichs, S. G. Wakeham, Intact polar lipids in the water column of the eastern tropical North Pacific: Abundance and structural variety of non-phosphorus lipids. *Biogeosciences* **15**, 6481–6501 (2018).
31. S. Ding *et al.*, Lipidomics of environmental microbial communities. II: Characterization using molecular networking and information theory. *Front. Microbiol.* **12**, 659315 (2021).
32. F. Schubotz, S. G. Wakeham, J. S. Lipp, H. F. Fredricks, K.-U. Hinrichs, Detection of microbial biomass by intact polar membrane lipid analysis in the water column and surface sediments of the Black Sea. *Environ. Microbiol.* **11**, 2720–2734 (2009).
33. G. Chwastek *et al.*, Principles of membrane adaptation revealed through environmentally induced bacterial lipidome remodeling. *Cell Rep.* **32**, 108165 (2020).
34. C. Klose *et al.*, Flexibility of a eukaryotic lipidome–Insights from yeast lipidomics. *PLoS One* **7**, e35063 (2012).
35. M. Y. Kellermann, M. Y. Yoshinaga, R. C. Valentine, L. Wörmer, D. L. Valentine, Important roles for membrane lipids in haloarchaeal bioenergetics. *Biochim. Biophys. Acta* **1858**, 2940–2956 (2016).
36. F. J. Elling, M. Könneke, M. Mußmann, A. Greve, K.-U. Hinrichs, Influence of temperature, pH, and salinity on membrane lipid composition and TEX_{86} of marine planktonic thaumarchaeal isolates. *Geochim. Cosmochim. Acta* **171**, 238–255 (2015).
37. T. A. Halamka *et al.*, Production of diverse brGDGTs by Acidobacterium *Solibacter usitatus* in response to temperature, pH, and O_2 provides a culturing perspective on brGDGT proxies and biosynthesis. *Geobiology* **21**, 102–118 (2023).
38. C. Cravo-Laureau, R. Matheron, C. Joulian, J.-L. Cayol, A. Hirschler-Réa, *Desulfatibacillum alkenivorans* sp. nov., a novel n-alkene-degrading, sulfate-reducing bacterium, and emended description of the genus *Desulfatibacillum*. *Int. J. Syst. Evol. Microbiol.* **54**, 1639–1642 (2004).
39. A. Vinçon-Laugier, C. Cravo-Laureau, I. Mitteau, V. Grossi, Temperature-dependent alkyl glycerol ether lipid composition of mesophilic and thermophilic sulfate-reducing bacteria. *Front. Microbiol.* **8**, 1532 (2017).
40. E. C. Hopmans *et al.*, Mono- to tetra-alkyl ether cardiolipins in a mesophilic, sulfate-reducing bacterium identified by UHPLC-HRMS^{n}: A novel class of membrane lipids. *Front. Microbiol.* **15**, 1404328 (2024).
41. N. J. Bale *et al.*, Lipidomics of environmental microbial communities. I: Visualization of component distributions using untargeted analysis of high-resolution mass spectrometry data. *Front. Microbiol.* **12**, 659302 (2021).
42. B. A. S. Van Mooy, G. Rocap, H. F. Fredricks, C. T. Evans, A. H. Devol, Sulfolipids dramatically decrease phosphorus demand by picocyanobacteria in oligotrophic marine environments. *Proc. Natl. Acad. Sci. U.S.A.* **103**, 8607 (2006).
43. D. Li, R. Halitschke, I. T. Baldwin, E. Gaquerel, Information theory tests critical predictions of plant defense theory for specialized metabolism. *Sci. Adv.* **6**, eaaz0381 (2020).
44. O. Martínez, M. H. Reyes-Valdés, Defining diversity, specialization, and gene specificity in transcriptomes through information theory. *Proc. Natl. Acad. Sci. U.S.A.* **105**, 9709 (2008).
45. B. Nowicka, J. Kruk, Occurrence, biosynthesis and function of isoprenoid quinones. *Biochim. Biophys. Acta* **1797**, 1587–1605 (2010).
46. M. Salvador-Castell, M. Tourte, P. M. Oger, In search for the membrane regulators of archaea. *Int. J. Mol. Sci.* **20**, 4434 (2019).
47. T. H. Haines, A new look at Cardiolipin. *Biochim. Biophys. Acta* **1788**, 1997–2002 (2009).
48. T. H. Haines, Anionic lipid headgroups as a proton-conducting pathway along the surface of membranes: A hypothesis. *Proc. Natl. Acad. Sci. U.S.A.* **80**, 160–164 (1983).
49. K. Venkatraman *et al.*, Cristae formation is a mechanical buckling event controlled by the inner mitochondrial membrane lipidome. *EMBO J.* **42**, e114054 (2023).
50. C. Klose, M. A. Surma, K. Simons, Organellar lipidomics–background and perspectives. *Curr. Opin. Cell Biol.* **25**, 406–413 (2013).
51. H. F. Sturt, R. E. Summons, K. Smith, M. Elvert, K.-U. Hinrichs, Intact polar membrane lipids in prokaryotes and sediments deciphered by high-performance liquid chromatography/electrospray ionization multistage mass spectrometry–new biomarkers for biogeochemistry and microbial ecology. *Rapid Commun. Mass Spectrom.* **18**, 617–628 (2004).
52. M. Kates, Influence of salt concentration on membrane lipids of halophilic bacteria. *FEMS Microbiol. Rev.* **2**, 95–101 (1986).
53. M. Kates, The phytanyl ether-linked polar lipids and isoprenoid neutral lipids of extremely halophilic bacteria. *Prog. Chem. Fats Other Lipids* **15**, 301–342 (1977).
54. J. S. Sinninghe Damsté *et al.*, 13, 16-Dimethyl octacosanedioic acid (iso-diabolic acid), a common membrane-spanning lipid of Acidobacteria subdivisions 1 and 3. *Appl. Environ. Microbiol.* **77**, 4147–4154 (2011).
55. I. M. López-Lara, O. Geiger, Bacterial lipid diversity. *Biochim. Biophys. Acta Mol. Cell Biol. Lipids* **1862**, 1287–1299 (2017).
56. O. Geiger, N. González-Silva, I. M. López-Lara, C. Sohlenkamp, Amino acid-containing membrane lipids in bacteria. *Prog. Lipid Res.* **49**, 46–60 (2010).
57. O. Geiger, V. Röhrs, B. Weissenmayer, T. M. Finan, J. E. Thomas-Oates, The regulator gene *phoB* mediates phosphate stress-controlled synthesis of the membrane lipid diacylglyceryl-N, N, N-trimethylhomoserine in *Rhizobium (Sinorhizobium) meliloti*. *Mol. Microbiol.* **32**, 63–73 (1999).
58. T. Bosak *et al.*, System-wide adaptations of *Desulfovibrio alaskensis* G20 to phosphate-limited conditions. *PLoS One* **11**, e0168719 (2016).

59. D. P. Lowenstein, K. Mayers, H. F. Fredricks, B. A. S. Van Mooy, Targeted and untargeted lipidomic analysis of haptophyte cultures reveals novel and divergent nutrient-stress adaptations. *Org. Geochem.* **161**, 104315 (2021).
60. Y. Okazaki *et al.*, A new class of plant lipid is essential for protection against phosphorus depletion. *Nat. Commun.* **4**, 1510 (2013).
61. A. F. Smith *et al.*, A novel class of sulfur-containing aminolipids widespread in marine roseobacters. *ISME J.* **15**, 2440–2453 (2021).
62. D. Roman *et al.*, Structure revision of a widespread marine sulfonolipid class based on isolation and total synthesis. *Angew. Chem. Int. Ed. Engl.*, 10.1002/anie.202401195 (2024).
63. T. Pluskal, S. Castillo, A. Villar-Briones, M. Oresič, MZmine 2: Modular framework for processing, visualizing, and analyzing mass spectrometry-based molecular profile data. *BMC Bioinformatics* **11**, 395 (2010).
64. L.-F. Nothias *et al.*, Feature-based molecular networking in the GNPS analysis environment. *Nat. Methods* **17**, 905–908 (2020).
65. M. Wang *et al.*, Sharing and community curation of mass spectrometry data with global natural products social molecular networking. *Nat. Biotechnol.* **34**, 828–837 (2016).
66. J. J. J. van der Hooft, J. Wandy, M. P. Barrett, K. E. V. Burgess, S. Rogers, Topic modeling for untargeted substructure exploration in metabolomics. *Proc. Natl. Acad. Sci. U.S.A.* **113**, 13738–13743 (2016).
67. M. Ernst *et al.*, MolNetEnhancer: Enhanced molecular networks by integrating metabolome mining and annotation tools. *Metabolites* **9**, 144 (2019).
68. K. Dührkop *et al.*, SIRIUS 4: A rapid tool for turning tandem mass spectra into metabolite structure information. *Nat. Methods* **16**, 299–302 (2019).
69. F. Huber *et al.*, Spec2Vec: Improved mass spectral similarity scoring through learning of structural relationships. *PLoS Comput. Biol.* **17**, e1008724 (2021).
70. J. Watrous *et al.*, Mass spectral molecular networking of living microbial colonies. *Proc. Natl. Acad. Sci. U.S.A.* **109**, E1743 (2012).
71. M. E. Smoot, K. Ono, J. Ruscheinski, P.-L. Wang, T. Ideker, Cytoscape 2.8: New features for data integration and network visualization. *Bioinformatics* **27**, 431–432 (2010).
72. P. Shannon *et al.*, Cytoscape: A software environment for integrated models of biomolecular interaction networks. *Genome Res.* **13**, 2498–2504 (2003).
73. S. Ding *et al.*, Changes in the membrane lipid composition of a *Sulfurimonas* species depend on the electron acceptor used for sulfur oxidation. *ISME Commun.* **2**, 121 (2022).
74. R. Lebret, R. Collobert, Word emdeddings through hellinger PCA. arXiv [Preprint] (2013). https://doi.org/10.48550/arXiv.1312.5542 (Accessed 4 January 2017).
75. D. Li, S. Heiling, I. T. Baldwin, E. Gaquerel, Illuminating a plant's tissue-specific metabolic diversity using computational metabolomics and information theory. *Proc. Natl. Acad. Sci. U.S.A.* **113**, E7610 (2016).
76. S. Ding *et al.*, Feature-Based-Molecular-Networking data from "Nitrogen and sulfur for phosphorus: Lipidome adaptation of anaerobic sulfate-reducing bacteria in phosphorus-deprived conditions." GNPS. https://gnps.ucsd.edu/ProteoSAFe/status.jsp?task=d62bea99758b4f48ba0fe1b294efec04. Deposited 19 September 2022.
77. S. Ding *et al.*, Mass spectrometry data from "Nitrogen and sulfur for phosphorus: Lipidome adaptation of anaerobic sulfate-reducing bacteria in phosphorus-deprived conditions." MASSIVE. https://doi.org/10.25345/C5TB0Z55N. Deposited 19 July 2023.
78. S. Ding *et al.*, Scripts from "Nitrogen and sulfur for phosphorus: Lipidome adaptation of anaerobic sulfate-reducing bacteria in phosphorus-deprived conditions." Zenodo. https://doi.org/10.5281/zenodo.10884543. Deposited 27 March 2024.